Spin current induced by in-plane magnetoelectric δ-barriers in a two-dimensional electron gas

S. G. Tan,[1] Mansoor B. A. Jalil,[2] and Thomas Liew[1,2]

[1]*Data Storage Institute, DSI Building, 5 Engineering Drive 1, (Off Kent Ridge Crescent), National University of Singapore, Singapore 117608*

[2]*Information Storage Materials Laboratory, Electrical and Computer Engineering Department, National University of Singapore, 4 Engineering Drive 3, Singapore 117576*

(Received 13 May 2005; revised manuscript received 15 August 2005; published 28 November 2005)

We model the ballistic spin current within a two-dimensional electron gas (2DEG) under the influence of magnetoelectric barriers and Rashba spin-orbit coupling. The magnetic field B_y is applied in the 2DEG in-plane direction rather than in the perpendicular direction B_z, as considered previously. The use of an in-plane field induces a spin current which is more resistant to the D'yakonov type of spin relaxation. It is shown theoretically that the electron energy dispersion is independent of the magnetic vector potential arising from in-plane fields. This enables electron conduction to maintain high conductance, even when multiple barriers are used to enhance the spin polarization of current. The polarization of current is also derived as a function of the Rashba spin-orbit coupling strength, the electric potential, and the magnetic field strength. The magnitude and direction of spin polarization can be modulated externally by a B_y field, which is useful for spintronics applications.

DOI: 10.1103/PhysRevB.72.205337 PACS number(s): 72.25.Hg

I. INTRODUCTION

It has been shown that in a two-dimensional electron gas (2DEG) based on III-V heterostructure, coherent transport of electrons in the ballistic regime can be manipulated by the application of external magnetic and electric fields.[1–6] The magnetic fields emanating from ferromagnetic gates on top of the 2DEG are highly localized and are usually approximated as δ functions (or δB field for short). In previous works, the δB fields were applied perpendicular to the 2DEG plane across the current conduction path. The differential transmission for spin-up and -down electrons through the series of magnetoelectric barriers results in the generation of spin-polarized current, with the reference spin axis in the vertical direction. In the drift-diffusion[7–9] regime, spin injection has been studied as a possible means to inject spin-polarized current from ferromagnetic contacts to the semiconductors. However, conductivity mismatch[7] suppresses spin injection.

Another contributory factor to the spin polarization of current comes from the conduction-band spin-orbit coupling (SOC) effects, experienced by electrons within a 2DEG in III-V-based semiconductors. These SOC effects arise from either surface inversion asymmetry (Rashba[10–12] effect) and or bulk inversion asymmetry (linear Dresselhaus[13,14] effect). However, these SOC effects also cause dephasing of spin currents polarized perpendicular to the 2DEG plane, via a D'yakonov-Perel'- (DP-) like mechanism. This spin depolarizing effect has not been considered in previous works which focused on perpendicular δB_z fields.

In this article, we propose the use of in-plane δB_y fields to harness the spin polarization potential of magnetoelectric barriers and SOC effects, while avoiding spin dephasing due to the DP-like mechanism. Our studies are illustrated with a model device which is based on the high-electron-mobility transistor (HEMT) heterostructure reminiscent of the Datta-Das[15] device, in which current flows within a 2DEG under the influence of δ magnetic fields applied through ferromagnetic gates, as shown in Fig. 1(a). Figure 1(b) is provided as a reference device for the application of perpendicular fields. Ferromagnetic gate stripes are patterned on top of the HEMT heterostructure consisting of a GaAs-AlGaAs layer. The magnetic field from the gates is approximated as a δ function of strength B_y. In calculating the spin polarization (P) ratio, we also neglect the effect of spin filtering at the

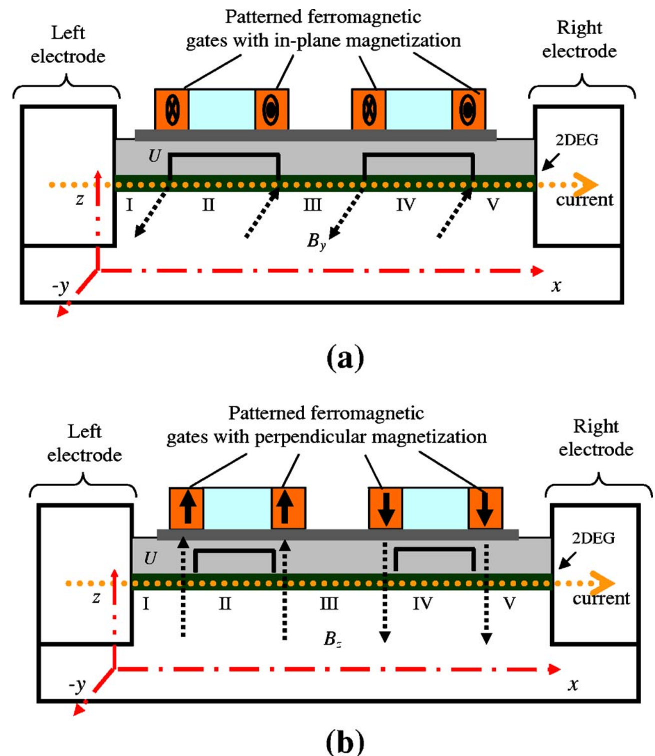

FIG. 1. (Color online) Schematic of the HEMT-type device with ferromagnetic gates deposited on top of the heterostructure, which produce (a) in-plane and (b) perpendicular magnetic (B) fields within the 2DEG plane.

 ©2005 The American Physical Society

ferromagnet-semiconductor boundaries (since this is strongly influenced by interfacial effects). Hence spin injection from ferromagnet to semiconductor and vice versa will not be considered in this paper.

II. THEORY

In the presence of an in-plane δB_y field, we can choose a corresponding Landau gauge of $A=(0,0,-A_z)$. The Hamiltonian that describes electron transport in a 2DEG in the presence of Rashba spin-orbit coupling and δ in-plane field is then given by

$$H = H_0 + H_C + H_R + H_Z + H_U = \frac{p_x^2}{2m^*} + \frac{p_y^2}{2m^*} + \frac{(p_z + eA_z)^2}{2m^*} + ezF_z + \eta_R(k_y\sigma_x - k_x\sigma_y) + \sigma_y\left(\frac{eg^*\hbar}{4m_0}\right)B_y\delta(0) + eU, \tag{1}$$

where H_0, H_C, H_R, H_Z, and H_U are terms corresponding to the kinetic energy, the intrinsic confining potential of the 2DEG, the Rashba effect, the Zeeman split, and the applied electric potential, respectively. $x=0$ is the position of the δ B_y field, while $m^*(m_0)$ is the electron's effective (real) mass, g^* the Lande factor, and $p_{x,y,z}$ the electron momentum in the x, y, z directions, respectively. In Eq. (1), the strength of the Rashba intreaction, which arises from the surface inversion asymmetry in the 2DEG, is given by $\eta_R=\alpha F_z$, where α is the Rashba parameter and F_z is confining electric field perpendicular to the 2DEG plane. Equation (1) can be expressed in the form of spinors (with the reference spin axis in the vertical z direction), and the eigenspinors of H are obtained by solving the 2×2 matrix equation of

$$\begin{bmatrix} H_0 + H_C + H_U & \eta_R k_y + i\,\eta_R[k_x - (\Lambda/\eta_R)] \\ \eta_R k_y - i\,\eta_R[k_x - (\Lambda/\eta_R)] & H_0 + H_C + H_U \end{bmatrix}\chi^{\pm} = E\chi^{\pm}, \tag{2}$$

where $\Lambda=(eg^*\hbar/4m_0)B_y$. The solutions to the eigenspinors are

$$\chi^{\pm} = \begin{pmatrix} \pm\dfrac{k_y + i[k_x - (\Lambda/\eta_R)]}{\sqrt{k_y^2 + [k_x - (\Lambda/\eta_R)]^2}} \\ 1 \end{pmatrix}, \tag{3}$$

where the correspnding eigenvalues are given by

$$E_T = H_0 + H_C + H_U \pm \eta_R\sqrt{k_y^2 + (k_x - \Lambda/\eta_R)^2}. \tag{3a}$$

Note that when electron motion is strictly one dimensional in the x direction (i.e., $k_y=0$), the eigenspinor is aligned parallel to the y axis. To simplify the wave function matching, we rotate the Cartesian spin axes such that the reference z axis coincides with the new axis parallel or antiparallel to the eigenspinors of Eq. (3) for a particular set of values of (B_y, η_R, k_y, k_x). Since the eigenspinors $\chi^{\pm}$ are oriented along the x-y plane, the spin rotation can be accomplished by transforming Eqs. (2) and (3) with a unitary matrix, $U(\theta=\pi/2,\phi)$, where ϕ is the azimuthal angle oriented along $\chi^{\pm}$. Because of symmetry, the energy eigenvalue obtained in the rotated frame due to H_R replicates that obtained in the original frame. Note that the rotation applies only to the spin, and not the spatial part of the total wave function. In this rotated frame, we can thus express the x dependence of the total wave function as

$$\psi_{\rm I}(x) = A^+e^{ik_1x}\begin{pmatrix}1\\0\end{pmatrix} + B^+e^{-iq_1x}\begin{pmatrix}1\\0\end{pmatrix} + A^-e^{iq_1x}\begin{pmatrix}0\\1\end{pmatrix} + B^-e^{-ik_1x}\begin{pmatrix}0\\1\end{pmatrix}, \tag{4}$$

$$\psi_{\rm II}(x) = C^+e^{ik_2x}\begin{pmatrix}1\\0\end{pmatrix} + D^+e^{-iq_2x}\begin{pmatrix}1\\0\end{pmatrix} + C^-e^{iq_2x}\begin{pmatrix}0\\1\end{pmatrix} + D^-e^{-ik_2x}\begin{pmatrix}0\\1\end{pmatrix}, \tag{5}$$

where I and II denote the regions shown in Fig. 1; $(+k_1, -k_1, +q_1, -q_1)$ and $(+k_2, -k_2, +q_2, -q_2)$ are the wave vectors corresponding to the four degenerate eigenfunctions of Eq. (3) in regions I and II, respectively, and are evaluated by considering Eq. (3a). The y dependence of the wave function is simply given by $\phi(y)=e^{ik_yy}$, due to the translation invariance in y, while the z dependence $\phi(z)$ of the wave function is determined by considering the confining potential of the 2DEG. In region I, we can express the total wave function of the system in the form of spinors as

$$\psi(x,y,z) = e^{ik_yy}\phi(z)\begin{pmatrix} A^+e^{ik_1x} + B^+e^{-iq_1x} \\ A^-e^{iq_1x} + B^-e^{-ik_1x}\end{pmatrix}. \tag{6}$$

To solve for $\phi(z)$ we approximate the confining potential as a triangular barrier. From the Hamiltonian, we obtain the following eigenvalue equation for $\phi(z)$:

$$\left[-\frac{\hbar^2}{2m^*}\phi''(z) - \frac{ie\hbar A_z}{m^*}\phi'(z) + \left(\frac{p_\parallel^2}{2m^*} + U + s\Lambda + H_R + \frac{e^2A_z^2}{2m^*}\right)\times\phi(z) + ezF_z\phi(z)\right] = E\phi(z). \tag{7}$$

The solution to the bound wave function $\phi(z)$ is given by a linear combination of Airy functions—i.e.,

$$\phi(z) = e^{-bz/2a}\,\mathrm{Ai}\left[\frac{b^2 + 4ac - 4aE_n + 4adz}{4a^{4/3}d^{2/3}}\right]C_1 + e^{-bz/2a}\,\mathrm{Bi}\left[\frac{b^2 + 4ac - 4aE_n + 4adz}{4a^{4/3}d^{2/3}}\right]C_2, \tag{8}$$

where C_1 and C_2 are constants and $a=\hbar^2/2m^*$, $b=ieA_z/m^*$, $d=eF_z$, and $c=\hbar^2(k_x^2+k_y^2)/2m^*+U+s\Lambda+H_R+e^2A_z^2/2m^*$. For the above solution to be a well-behaved function as $z\to\infty$, we need $C_2=0$. To determine the subband energies within the 2DEG potential well, we consider the boundary condition of $\phi(z=0)=0$, where $z=0$ is taken to be the conduction-band minimum of the 2DEG in the z direction. Noting that

$$\phi(z) = e^{-bz/2a}\,\mathrm{Ai}\left[\frac{b^2+4ac-4aE_n+4adz}{4a^{4/3}d^{2/3}}\right]c_1$$

has roots -2.338, $-4.088, \ldots$ the lowest subband energy is thus given by

$$E_n = (b^2/4a) + c + 2.338a^{1/3}d^{2/3}, \tag{9}$$

i.e.,

$$E_n = \frac{\hbar^2(k_x^2+k_y^2)}{2m^*} + U + s\Lambda + H_R + 2.338\left(\frac{(eF_z\hbar)^2}{2m^*}\right)^{1/3}. \tag{10}$$

At low temperatures, transport in the 2DEG is dominated by electrons at the Fermi level, so that $E_n = E_F$ (Fermi energy). It is interesting to note that in the triangular barrier approximation, the subband energy

$$E_{\mathrm{sub}} = 2.338(eF_z)^{2/3}/(2m^*)^{1/3}$$

of Eq. (10) is independent of the gauge A_z and hence of the magnetic field B_y. Thus, E_{sub} can be absorbed into the variable U in Eq. (10) to give U_{eff}.

It has been discussed that in the case of δB_z fields (perpendicular to 2DEG plane), multiple barriers need to be used to attain high spin polarization P. However, the presence of multiple barriers tends to suppress the overall transmission probability (T) because each barrier contributes to ΔA_y across the conducting path and reduces the kinetic energy in the propagation direction. In the in-plane B_y case, however, Eq. (10) shows that the wave vector k_x in the propagation direction is unaffected by any increase in A_z. Thus, the use of higher B_y fields or multiple δ-field barriers with the strength of B_y each can act to increase P of the spin current without lowering the device conductance. From Eq. (11), the propagation wave vector k_x is given by

$$k_x^2 = \left[-s\eta_R\frac{m}{\hbar^2} \pm \sqrt{\left(\eta_R\frac{m}{\hbar^2}\right)^2 + \frac{2m}{\hbar^2}(E-U_{eff})}\right]^2 - k_y^2. \tag{11}$$

In region I of Fig. 1 (where $U_{eff}=0$), the four solutions for the wave vector (k_x) are given by

$$+k_1 \equiv \sqrt{(f+\sqrt{g})^2 - k_y^2}, \quad -k_1 \equiv -\sqrt{(-f-\sqrt{g})^2 - k_y^2}, \tag{12}$$

$$+q_1 \equiv \sqrt{(-f+\sqrt{g})^2 - k_y^2}, \quad -q_1 \equiv -\sqrt{(f-\sqrt{g})^2 - k_y^2}, \tag{13}$$

where $f = \eta_R m/\hbar^2$ and $g = (\eta_R m/\hbar^2)^2 + (2m/\hbar^2)(E)$. In region II, g is replaced by $g' = (\eta_R m/\hbar^2)^2 + (2m/\hbar^2)(E-U_{eff})$; k_1, q_1 are denoted by k_2, q_2, respectively. Having determined the wave vector k_x, we now solve for the electron wave function by (i) matching the amplitude of the wave function and (ii) ensuring flux continuity at the boundaries marked by the δB_y fields (see Fig. 1). By considering the spinor wave functions in regions I and II as shown in Eqs. (4) and (5), respectively, we obtained the following from wave function matching:

$$\begin{pmatrix} A^+ + B^+ \\ A^- + B^- \end{pmatrix} = \begin{pmatrix} C^+ + D^+ \\ C^- + D^- \end{pmatrix}. \tag{14}$$

To derive the flux continuity relation for each spin across a boundary, we integrate the one-dimensional Schrödinger equation over a small range $[+\xi, -\xi]$ along x, on either side of the boundary—i.e.,

$$\lim_{\xi\to 0}\left[\int_{-\xi}^{+\xi}\left(\frac{p_x^2}{2m^*} + \eta_R k_B \sigma_z\right)\begin{pmatrix}\psi^+\\ \psi^-\end{pmatrix}dx\right] = \int_{-\xi}^{+\xi} E\begin{pmatrix}\psi^+\\ \psi^-\end{pmatrix}dx, \tag{15}$$

where $k_B = \sqrt{k_y^2 + (k_x - \Lambda/\eta_R)^2}$. Solving Eq. (15) leads to

$$\frac{-i\hbar^2}{2m^*}\left[\begin{pmatrix} k_2C^+ - q_2D^+ \\ q_2C^- - k_2D^- \end{pmatrix} - \begin{pmatrix} k_1A^+ - q_1B^+ \\ q_1A^- - k_1B^- \end{pmatrix}\right] + \eta_R\int_{-\xi}^{+\xi}\begin{pmatrix} \sqrt{k_y^2 + [k_x - (\Lambda/\eta_R)]^2}\,\psi^+ \\ \sqrt{k_y^2 + [k_x - (\Lambda/\eta_R)]^2}\,\psi^- \end{pmatrix}dx = 0. \tag{16}$$

Solving Eq. (16) explicitly (in the limit of $\xi \to 0$) results in the relation

$$\left(\frac{-i\hbar^2}{2m^*}\right)\begin{pmatrix} k_2C^+ - q_2D^+ \\ q_2C^- - k_2D^- \end{pmatrix} - \left(\frac{-i\hbar^2}{2m^*}\right)\begin{pmatrix} k_1A^+ - q_1B^+ \\ q_1A^- - k_1B^- \end{pmatrix} + \begin{pmatrix} \psi^+(0)\Lambda \\ -\psi^-(0)\Lambda \end{pmatrix} = 0. \tag{17}$$

In obtaining Eq. (17), we note that as the range of integration approaches zero, only the term ($\Lambda\psi^{\pm}$) which contains the δ function term $\delta(0)$ will yield a finite contribution. The resulting transfer matrices linking the wave functions in regions I and II are then given by

$$\begin{bmatrix} A^+ \\ B^+ \end{bmatrix} = \begin{bmatrix} \dfrac{q_1+k_2+i\vartheta}{k_1+q_1} & \dfrac{q_1+q_2+i\vartheta}{k_1+q_1} \\ \dfrac{k_1-k_2-i\vartheta}{k_1+q_1} & \dfrac{k_1-q_2-i\vartheta}{k_1+q_1} \end{bmatrix} \cdot \begin{bmatrix} C^+ \\ D^+ \end{bmatrix}, \tag{18a}$$

$$\begin{bmatrix} A^- \\ B^- \end{bmatrix} = \begin{bmatrix} \dfrac{k_1+q_2-i\vartheta}{k_1+q_1} & \dfrac{k_1-k_2-i\vartheta}{k_1+q_1} \\ \dfrac{q_1-q_2+i\vartheta}{k_1+q_1} & \dfrac{q_1+k_2+i\vartheta}{k_1+q_1} \end{bmatrix} \cdot \begin{bmatrix} C^- \\ D^- \end{bmatrix}, \tag{18b}$$

where $\vartheta = (m^*/m_0)eg^*B_y/$. Assuming the wave function in region II has no reflection component, the transmission probability through the δ barrier is given by

$$T^+ = \frac{k_2}{k_1}\left|\frac{C^+}{A^+}\right|^2, \quad T^- = \frac{q_2}{q_1}\left|\frac{C^-}{A^-}\right|^2. \tag{19}$$

The spin polarization P is then given by

$$P = \frac{T^{+} - T^{-}}{T^{+} + T^{-}} = \frac{q_1 k_2 |k_1 + q_2 - i\vartheta|^2 - k_1 q_2 |q_1 + k_2 + i\vartheta|^2}{q_1 k_2 |k_1 + q_2 - i\vartheta| + k_1 q_2 |q_1 + k_2 + i\vartheta|^2}. \quad (20)$$

Using Eqs. (12) and (13) and the corresponding expressions for wave vectors in region II, the explicit expression for P for conductance mode of $k_y=0$ can be simplified to

$$P = \frac{(q_1 k_2 - k_1 q_2)[(\sqrt{b} + \sqrt{c})^2 + \vartheta^2]}{(q_1 k_2 + k_1 q_2)[(\sqrt{b} + \sqrt{c})^2 + \vartheta^2]} = \frac{(q_1 k_2 - k_1 q_2)}{(q_1 k_2 + k_1 q_2)}. \quad (21)$$

Equation (21) shows that when $k_y=0$, the in-plane B_y field does not contribute to the strength of P along the spin quantization axis (y) for the spin current. For nonzero k_y, B_y might have a contribution to P through ϑ as shown in Eq. (20). However, the important point here is that the application of B_y plays the role of aligning the spin quantization axis closer to the y axis, as can be deduced from the eigenspinor of Eq. (3). For quantization axis closer (farther) to the original y axis, spin projection in the y axis (P_y) increases (decreases) accordingly, providing a means for spin current modulation. Therefore, for zero or nonzero k_y, B_y provides an external means of controlling P_y. In this system, the switching of B_y field also switches the P of spin current in y, thus modulating the resistance through a magnetized contact. Thus the switching of B_y field provides a feature similar to nonvolatile storage.

III. DISCUSSION

A. Conceptual advantages

We have conceived and derived equations that describe spin-dependent transport within a 2DEG in the ballistic regime under the influence of in-plane magnetoelectric barriers and spin-orbit coupling induced by surface inversion asymmetry. From our analysis, we can list several significant advantages for the application of in-plane B fields as opposed to the out-of-plane fields considered previously in Refs. 1–6. First of all, the application of multiple magnetic barriers or increasing strength of B_y in order to maximize the spin polarization P will not lower the probability of electron transmission across the barriers, as had been previously discussed in Refs. 16–18. This is because in the case of the in-plane fields, the energy dispersion equation of Eq. (10) is independent of B_y and the corresponding magnetic vector potentials of A_z. In the case of out-of-plane fields, however, A_y is coupled to k_y in the dispersion relation, and this results in additional energy cost to the total available (kinetic) energy for electron transmission. It has been previously suggested that the zero-A (Ref. 16) type of B-field configurations should be used in the case of perpendicular fields, in order to achieve a high net P of spin current at reasonably high conductance. However, this will entail the use of more B_z barriers and/or of greater strength, thus rendering the device less suitable for small-cell, high-density applications like memory.

Furthermore, since the transport system is ballistic, it is necessary to ensure that the entire electron conduction path is shorter than the spin relaxation length associated with the spin-orbit mechanism. The use of in-plane fields eliminates the need for zero-A configuration which requires multiple barriers within a double-pair element[16,18] to achieve high current polarization at high conductance. In the case of in-plane fields, the active electron conduction length can be greatly reduced, making it easier to achieve the ballistic condition assumed in the calculations.

The spin current induced by the in-plane field is also more resistant to the D'yakonov-like spin scattering effects. This spin scattering, which arises from spin-orbit coupling, has a detrimental effect on the polarization P of spin current across a 2DEG with an out-of-plane field B_z. This is because the effective in-plane magnetic field of the Rashba spin orbit causes the electron spin (polarized along $\pm z$) to precess about an axis in the x-y plane, leading to spin dephasing in a similar way to the D'yakonov-Perel[19] mechanism. Previous works[1–4] have neglected this source of spin relaxation and thus may have overestimated the spin polarization which can be achieved. By contrast, if we use a δ-function B_y field, the eigenspinor direction (total field) and the effective field direction due to the in-plane spin-orbit coupling differs only by the azimuthal angle in the x-y plane. Hence, the spin state even when averaged over the entire precessional orbit will still have a component in the eigenspinor direction, thus reducing the effect of the D'yakonov spin relaxation mechanism.

Finally, from our analysis we found that for the in-plane field case, the spin polarization P of current is a function of the Rashba spin-orbit strength and the electric potential, whereas the spin quantization axis (eigenspinor direction) varies in the azimuthal direction with the strength of the delta B_y field. The stronger the δ-field strength, the closer is the quantization axis to the y axis of the original frame. The availability of parameters which affect different aspects of the spin polarization of current (in terms of magnitude and direction) confers versatility for spintronics device applications.

B. Numerical simulations and applications

To demonstrate the above-mentioned advantages, we performed a numerical simulation of spin-dependent transmission through the magnetoelectric δ barriers. We consider a GaAs 2DEG system, as shown in Figs. 1(a) and 1(b), in our calculations. For numerical convenience, all parameters are reduced to dimensionless units in the following manner: $x \to l_B x$, $E \to \omega_C E$, $l_B = \sqrt{/eB_0}$, and $\omega_C = eB_0/m^*$. Here B_0 is an arbitrary, but commonly achievable magnetic-field strength in a practical device. In standard 2DEG GaAs, material parameters are as follows: $m^*=0.067m_0$, $g^*=0.44$, and $g=0.0295$; for $B_0=0.2$ T, $l_B=57$ nm, and $E_0=0.34$ meV. The Rashba parameter in GaAs is assumed to have a typical value of $0.2E_0 l_B$ or approximately 5.8×10^{-12} eV m, while the Fermi energy E_F is taken to be $10E_0$ (3.4 meV), which corresponds to a 2DEG carrier density of $\sim 10^{11}$ cm^{-2}. The device is operated by applying a combination of electrical and magnetic barriers across the 2DEG. The electric potentials U of $(+2,-2)E_0$ are applied to the two gate electrodes which

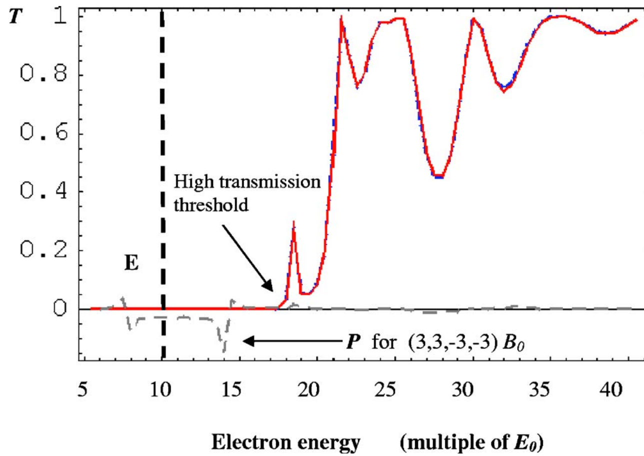

FIG. 2. (Color online) Transmission probability as a function of electron energy for the case of perpendicular B_z field configuration of $(+3,+3,-3,-3)B_0$. The transmission threshold is shifted to the high-energy region way beyond the Fermi energy (denoted by the vertical dotted line). At the Fermi level, the transmission probability and hence conductance for both spins are close to zero, although there is spin polarization of current.

correspond to regions II and IV, respectively, of the electron conduction path of Figs. 1(a) and 1(b). For the case of perpendicular B fields, a magnetic field configuration of $(+3,+3,-3,-3)B_0$ is established across the electron conduction path, as shown in Fig. 1(b). Ideally the gates should all be magnetized in one direction to increase the spin polarization P, but this will have the undesired effect of pushing the transmission threshold way beyond E_F. The calculated electron transmission (T) and spin polarization (P) are plotted in Fig. 2. The threshold for appreciable T is still about twice that of E_F at $20E_0$. For electron energy less than E_F, P is at most about 7% while the transmission T is close to zero. This is undesirable from a practical standpoint, since at normal operating temperature most conduction electrons have energies close to or lower than E_F. It has been previously suggested[16–18] that increasing the number of barriers could increase P, but this has the adverse effects of pushing the T threshold further into the high-energy region. We now calculate the corresponding T and P profiles for the device with in-plane magnetic fields as shown in Fig. 1(a). For this device we can apply an all-parallel, B-field configuration of $(+3,+3,+3,+3)E_0$ since the resulting increase in A will not lower the wave vector in the propagation direction [as can be seen from Eq. (3)], unlike for the perpendicular-field device of Fig. 1(b). The T and P profiles are plotted in Fig. 3. Compared to the corresponding curves in Fig. 2 for the perpendicular-field device, the T threshold is significantly lower and high T values are attained in the low-energy region ($E < E_F$). The average P value in this energy range has also been increased slightly to about 3%–10%. Since the net gain in A has no effect on the T threshold, we are able to apply all-parallel fields of greater strength, in order to enhance P. Thus, in Fig. 4 we plot the calculated T and P curves corresponding to an in-plane B field configuration of $(+9,+9,+9,+9)B_0$. The plots show that the higher B field strength has increased P to above 20% in the sub-Fermi-energy range, without shifting the T threshold to higher energies. We can thus conclude that in the in-plane field device, the spin polarization P can be maximized by increasing the number and strength of B-field barriers, which are arranged in an all-parallel configuration. This is due to the fact that for the in-plane field configuration, the wave vector in the propagation direction is decoupled from A [Eq. (3)] and this thus lowers the transverse energy cost[16–18] for electron transmission with increasing B-field barrier number and strength.

One important application of the in-plane B-field device is to serve as a source of spin-polarized current, which is one of the crucial requirements of spintronics. Furthermore, the degree of spin polarization of the current within the 2DEG can be modulated externally by applying B and U fields on the ferromagnetic gates of the device. Our numerical calculations have shown that increasing the B-field strength increases the spin polarization, without suppressing the electron transmission at or below E_F. This device has thus removed a fundamental cap to the strength of the magnetic fields which can be applied. The application of strong B fields to induce highly spin-polarized current is only now limited only by the engineering challenge of generating those

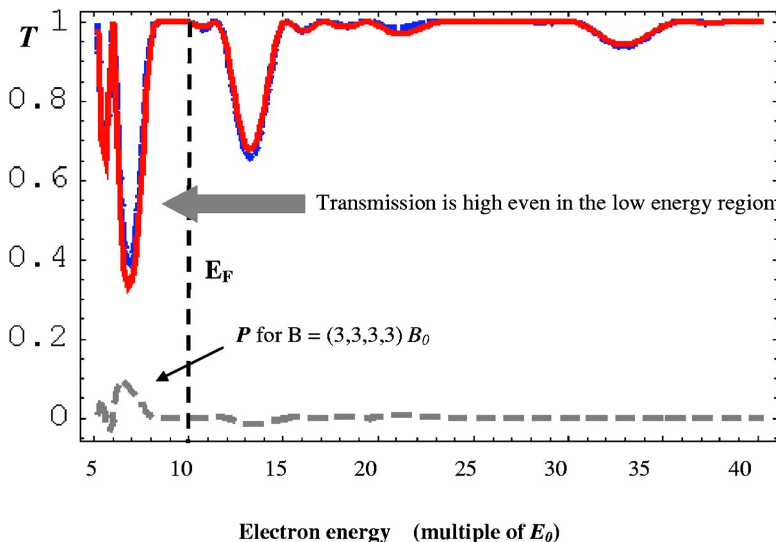

FIG. 3. (Color online) Transmission probability as a function of electron energy for the case of in-plane B_y fields having the all-parallel configuration of $(+3,+3,+3,+3)B_0$. Compared to Fig. 2, the transmission threshold has not shifted to the high-energy region beyond the Fermi level E_F. At E_F, the transmission is almost 100% for electron of both spins, and hence conductance is high. The all-parallel fields result in a peak spin polarization of about 10%.

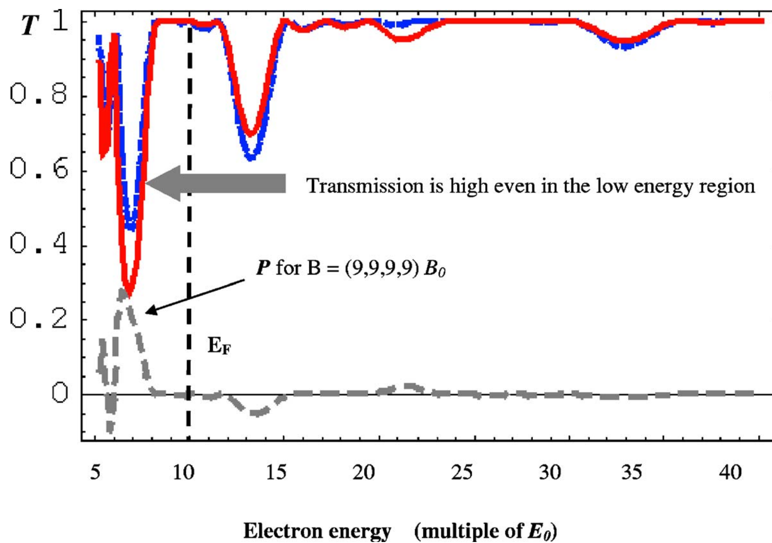

FIG. 4. (Color online) Transmission probability as a function of electron energy for the case of high in-plane B_y fields having the all-parallel configuration of $(+9,+9,+9,+9)B_0$. As in Fig. 3, the transmission threshold is not shifted to the high-energy region, and at E_F transmission is close to 100% for electron of both spins. However, the peak spin polarization is much higher at about 30%.

high fields in the device. These difficulties can be overcome with material and device design, and optimization of the spatial field distribution.

The in-plane field device system can also be made to function as a spin transistor since the strength of the spin polarization of current can be converted to a measurable resistance change by contacting the device to ferromagnetic source-drain electrodes. Spin-based transistors based on other schemes have been proposed previously, such as the HEMT-based device with ferromagnetic gates,[1–6] the spin-injection device,[7–9] the Rashba spin-orbit coupling device,[12,15,20,21] the Dresselhaus spin-orbit coupling device,[22,23] and the magnetic tunneling transistors (MTT).[24,25] It has been argued, both theoretically and experimentally, that such spin-based transistors can conceivably be a viable alternative to conventional metal-oxide-semiconductor field-effect transistors (MOSFET's) due to their lower power consumption and higher speed. However, there are many obstacles to the practical implementation of the various spin transistor schemes. For instance, those based on spin injection devices face the fundamental problem of conductivity mismatch that suppresses spin polarization in the semiconductor, while the MTT devices can be adversely affected by the quality of Schottky barriers as well as other interfacial effects. The Rashba and Dresselhaus spin-orbit coupling devices are limited by their low operating temperature. Furthermore, the electron spin state in these spin-orbit coupling devices is coupled to the momentum state, which makes it essential to restrict the electron motion to selected momentum states. The requirement to confine the electron motion poses an additional challenge to fabricating a viable device based on these principles. Recent analyses[26] have also shown that transistors utilizing the spin-orbit coupling effect require a longer channel length than previously thought, which makes it difficult to achieve the necessary ballistic transport. By contrast 2DEG spin transistor with in-plane magnetic fields has an additional control parameter—i.e., the applied δ in-plane fields. The total effective magnetic fields can thus be tuned to focus closer to the applied delta in-plane field. It also can function at a higher temperature, since they are now more resistant to the D'yakonov spin relaxation mechanism, which typically increases with temperature. Compared to spin-injection-based transistors and MTT devices, the in-plane ferromagnetic transistor devices are also

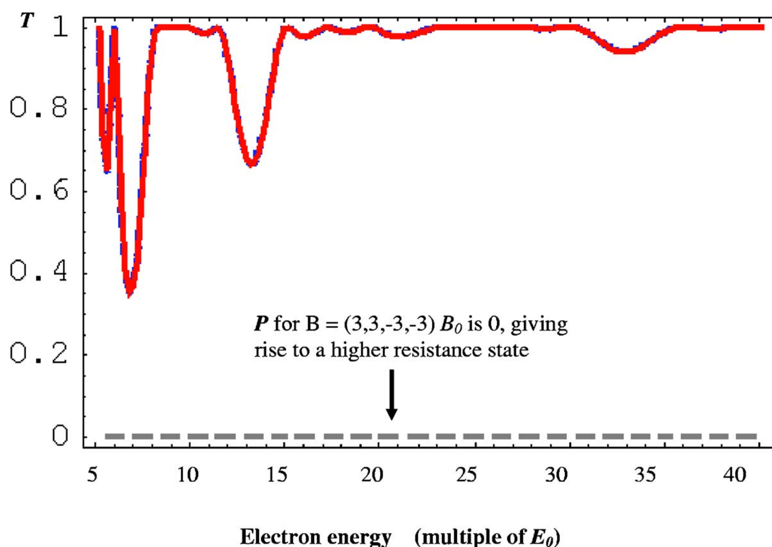

FIG. 5. (Color online) Transmission probability as a function of electron energy for the case of in-plane B_y field configuration of $(+3,+3,-3,-3)B_0$. This results in zero spin polarization at all electron energies and thus corresponds to a high-resistance state in the 2DEG channel.

less susceptible to interfacial effects since the spin polarizing effect by the magnetoelectric barriers occurs away from the interfaces.

Finally, as we have shown recently,[27,28] a 2DEG HEMT device with ferromagnetic gates in the perpendicular B-field configuration can be adapted for use as a single-transistor nonvolatile storage. Our calculations reveal that with the application of in-plane B fields, this device could perform this function even better. To show this, we consider an antiparallel configuration with fields pointing in the positive and negative in-plane directions—i.e., $(+B,+B,-B,-B)$—and calculate the T and P profiles, as plotted in Fig. 5. We find that this antiparallel configuration produces zero polarization of spin current for all electron energies. By contrast in Figs. 3 and 4, with an all-parallel magnetic field configuration, we obtain an appreciable spin polarization, especially with higher field strength (Fig. 4). These two distinct states—zero P for antiparallel and high P for all-parallel configuration—can be differentiated by converting them into resulting high- and low-resistance states of the device, if we were to connect the device to ferromagnetic source-drain electrodes. The high- and low-resistance states could then be used to represent nonvolatile binary memory states, just as in a conventional magnetoresistive random access memory (MRAM).

IV. CONCLUSION

In conclusion, we have analytically derived the electron energy dispersion and spin polarization current in a 2DEG HEMT device under the application of in-plane magnetic fields from ferromagnetic (FM) gate elements. We have also supported our analysis with numerical simulations. Based on our numerical and analytical analysis, we deduced several distinct advantages of the in-plane B-field configurations, compared to the out-of-plane B-field configuration considered in previous works. We show that these advantages contribute to the prospects of realizing several spintronic devices such as the spin current source and a spin-based transistor. We also conceive a specific adaptation of this 2DEG HEMT device with FM gates, which can perform the function of nonvolatile storage.

[1] Amlan Majumdar, Phys. Rev. B **54**, 11911 (1996).
[2] Yong Guo, Binglin Gu, Wenhui Duan, and Yu Zhang, Phys. Rev. B **55**, 9314 (1997).
[3] G. Papp and F. M. Peeters, Appl. Phys. Lett. **78**, 2184 (2001).
[4] H. Z. Xu and Y. Okada, Appl. Phys. Lett. **79**, 3119 (2001).
[5] Y. Jiang, M. B. A. Jalil, and T. S. Low, Appl. Phys. Lett. **80**, 1673 (2002).
[6] Yong Guo, Jian-Hua Qin, Xn-Yi Chen, and Bing-Lin Gu, Semicond. Sci. Technol. **18**, 297 (2003).
[7] G. Schmidt, D. Ferrand, L. W. Molenkamp, A. T. Filip, and B. J. van Wees, Phys. Rev. B **62**, R4790 (2000).
[8] E. I. Rashba, Phys. Rev. B **62**, R16267 (2000).
[9] A. Fert and H. Jaffres, Phys. Rev. B **64**, 184420 (2001).
[10] Jun-ichiro Inoue, Gerrit E. W. Bauer, and Laurens W. Molenkamp, Phys. Rev. B **67**, 033104 (2003).
[11] E. I. Rashba and Al. L. Efros, Phys. Rev. Lett. **91**, 126405 (2003).
[12] Laurens W. Molenkamp, G. Schmidt, and Gerrit E. W. Bauer, Phys. Rev. B **64**, 121202(R) (2001).
[13] John Schliemann and Daniel Loss, Phys. Rev. B **68**, 165311 (2003).
[14] G. Dresselhaus, Phys. Rev. **100**, 580 (1955).
[15] Supriyo Datta and Biswajit Das, Appl. Phys. Lett. **56**(7), 665 (1989).
[16] M. B. A. Jalil, S. G. Tan, T. Liew, K. L. Teo, and T. C. Chong, J. Appl. Phys. **95**, 7321 (2004).
[17] K. C. Seo, G. Ihm, K.-H. Ahn, and S. J. Lee, J. Appl. Phys. **95**, 7252 (2004).
[18] M. B. A. Jalil, J. Appl. Phys. **97**, 024507 (2005).
[19] M. I. D'yakonov and V. I. Perel', Zh. Eksp. Teor. Fiz. **60**, 1954 (1971) [Sov. Phys. JETP **33**, 1053 (1971)].
[20] Takaaki Koga, Junsaku Nitta, Tatsushi Akazaki, and Hideaki Takayanagi, Phys. Rev. Lett. **89**, 046801 (2002).
[21] J. Nitta, T. Akazaki, H. Takayanagi, and T. Enoki, Phys. Rev. Lett. **78**, 1335 (1997).
[22] V. I. Perel', S. A. Tarasenko, I. N. Yassievich, S. D. Ganichev, V. V. Bel'kov, and W. Prettl, Phys. Rev. B **67**, 201304(R) (2003).
[23] S. G. Tan, M. B. A. Jalil, Thomas Liew, K. L. Teo, and T. C. Chong, J. Appl. Phys. **97**, 10D506 (2005).
[24] Kap Soo Yoon, Jung Yup Yang, Ki Woong Kim, Ja Hyun Koo, Chae Ok Kim, and Jin Pyo Hong, J. Appl. Phys. **95**, 6933 (2004).
[25] Sebastiaan van Dijken, Xin Jiang, and Stuart S. P. Parkin, Appl. Phys. Lett. **80**, 3364, (2002).
[26] S. Bandyopadhyay and M. Cahay, Appl. Phys. Lett. **85**, 1433 (2004).
[27] S. G. Tan, M. B. A. Jalil, Thomas Liew, K. L. Teo, G. H. Lai, and T. C. Chong, J. Supercond. (to be published).
[28] S. G. Tan, M. B. A. Jalil, Vimal Kumar, Thomas Liew, K. L. Teo, and T. C. Chong, in Proceedings of the 3rd International Conference on Materials for Advanced Technologies, Singapore [Thin Solid Films (to be published)].